Journal of Materials Chemistry C

Accepted Manuscript

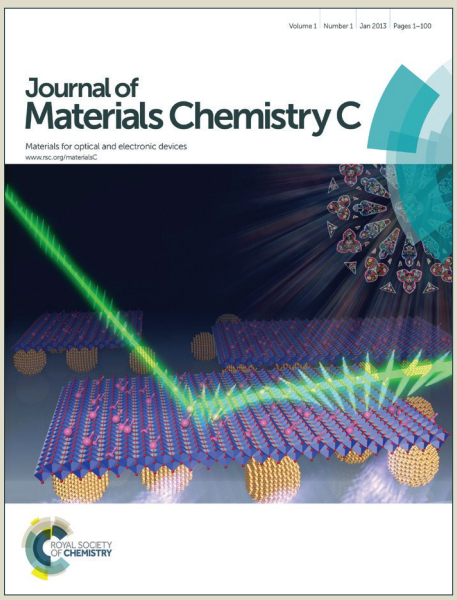

ROYAL SOCIETY OF CHEMISTRY

www.rsc.org/materialsC

Journal Name

ARTICLE

The influence of inner electric field on the performance of three types of Zn-porphyrin sensitizers in dye sensitized solar cells: A theoretical study

Received 00th January 20xx,
Accepted 00th January 20xx

DOI: 10.1039/x0xx00000x

www.rsc.org/

Miao Xie,[ab] Fu-Quan Bai, *[a] Hong-Xing Zhang[a] and Yue-Qing Zheng*[b]

It is well-known that the inner electric field formed between the counter electrode and the semiconductor surface has a substantial effect on the efficiencies of dye-sensitized solar cells (DSSCs). To reveal the function of inner electric field for different types of porphyrin sensitizers in DSSCs, the properties of three types of porphyrin sensitizers (a, β, and center axial positions) under different electric fields were calculated by using density functional theory (DFT) and time dependent density functional theory (TD-DFT). The electronic structures and optical properties of these studied dyes in tetrahydrofuran (THF) solution were also investigated correspondingly. Key parameters of the short-circuit current density (J_{sc}) including light harvesting efficiency (*LHE*), electron injection driving force (ΔG_{inject}) and intramolecular charge transfer (ICT) were detailedly discussed. The results show that the a-position type porphyrin sensitizer can be used as a potential sensitizer for DSSCs under enhanced electric field. We expect the present study would deepen the understanding of the function of inner electric field and may be helpful in DSSCs design in the future.

1. Introduction

As alternatives to conventional silicon-based inorganic solar cells, dye-sensitized solar cells (DSSCs) have low production costs, simple fabrication, low toxicity of the constituent elements and relatively high light-to-electric energy conversion efficiencies (η) especially under low-light intensities and scattered light conditions.[1-3] As important components in DSSCs, sensitizers play a crucial role in promoting a higher solar-to-electricity conversion efficiency. Several sensitizers, such as ruthenium complexes,[4-6] zinc porphyrin[7, 8] and metal-free organic dyes[9, 10] have shown high DSSC efficiency. Among these sensitizers, porphyrin sensitizers have been considered to be promising candidates for DSSCs due to their stable structure, intense Soret and Q bands and tunable spectral properties. Recently, the cobalt redox-based DSSCs may reach a conversion efficiency of exceeding 12% (12.3% with YD2-o-C8 dye[7] and 13% with SM315 dye[8]). These milestones stimulate the investigation of porphyrin sensitizers for developing high-efficiency DSSCs.

In order to be applied to DSSC device, porphyrin sensitizers must have anchoring group or bridged-binding group in their molecular structures, which allow the attachment of the dye to the TiO_2 surface.[11] Therefore, different dyes can be designed by adopting different connecting positions of the anchoring groups. In general, there are four meso and eight β-positions in a free based porphyrin macrocycle. Moreover, taking metal-porphyrin into account, its metal axial center of metal-porphyrin can also provide two connection sites (one of them headed towards the effect connection with TiO_2). All these above-mentioned positions are potentially available for functionalizations with at least one anchoring groups or other substituents (see Scheme 1). Hence, according to the connection position of the acceptor group, porphyrin sensitizers can be divided into three types (meso,[7, 8] β,[4, 12, 13] and center axial positions[14-16]) according to the connection position of the acceptor group. Nevertheless, the efficiencies of them are greatly different. Among these different porphyrin sensitizers, the meso-porphyrins have been the most efficient reported in DSSCs. In 2014, Nazzeruddin and co-workers reported the meso-porphyrins dye SM315 achieving a power conversion efficiency 13%.[8] Besides, for β-substituted porphyrin sensitizers, to date the tda-2b-bd-Zn dye reported by Ishida et al. in 2011 achieve the best performance with a power conversion efficiency of 7.5% to date.[12] Lastly, non-covalent self-assembled systems of metal-porphyrin through axial coordination linked center axial position still belongs to porphyrin sensitizers in DSSCs. This type of sensitizer is less efficient than that mentioned above.

However, the understanding of DSSCs complex system is still far from percipient. And, the performance of dye sensitizer is affected by many factors. The detailed principle of operation for DSSCs is still very necessary to identify the factors that

[a] Institute of Theoretical Chemistry, Jilin University, Changchun 130023, People's Republic of China. E-mail: baifq@jlu.edu.cn (Fu-Quan Bai).
[b] Research Center of Applied Solid State Chemistry, Chemistry Institute for Synthesis and Green Application, Ningbo University, Ningbo 315211, P.R. China
*E-mail: zhengcm@nbu.edu.cn (Yue-Qing Zheng)

† Footnotes relating to the title and/or authors should appear here.
Electronic Supplementary Information (ESI) available: [details of any supplementary information available should be included here]. See DOI: 10.1039/x0xx00000x

actually limit their performance. Actually, when the DSSCs work, the electron-injection of photo-excited dye and regeneration of redox mediator processes occur, thus leading to a large number of electrons accumulations in TiO_2 semiconductor and the counter electrode. Consequently, it is inevitable that the inner electric field is created between TiO_2 semiconductor and counter electrode under sunlight condition, which will affect the efficiency of dyes during the operation of DSSCs, further determine the overall performance of DSSCs to some extent. Previous experimental and theoretical studies were reported that the reversible or local electric field affects the absorption spectra of the sensitizer in DSSCs.[17-19] Boschloo et al. observed the change in the absorption spectra of attached ID28, D149 and P1 sensitizer molecules.[20, 21] They interpreted that these appearances could be caused by a band edge shift of the TiO_2 semiconductor in these devices and/or a shift of the redox potential of the electrolyte. Yang and co-works reported the interaction between accumulated electrons inside TiO_2 and the cations in the surrounding electrolyte are at the TiO_2/dye/electrolyte interface.[22] They found the slow local charge compensation and a reversible electric field during the local charge compensation processes at these interfaces. In addition, for the theoretical study of the local electric field between dye and TiO_2 surface, our group investigated that the lower the electric field strength could lead to the better performance of DSSCs.[17] Inspired by the above researches, we speculate whether inner electric field acting on ground-state sensitizer molecules could provide a clear explanation on the greatly different efficiencies of various porphyrin-sensitizers.

Thus in the present study, we constructed a D-π-A model containing TiO_2 substrate and three types of Zn-porphyrin sensitizers as shown in Scheme 1. Aiming to elucidate how the inner electric field of the DSSCs affects the dipole moment and the absorption spectra of these three studied types Zn-porphyrin sensitizers, exhibit the property of short-circuit photocurrent density and open-circuit photo-voltage under different electric field strengths, and thus improve our comprehension of dye molecular engineering in DSSCs.

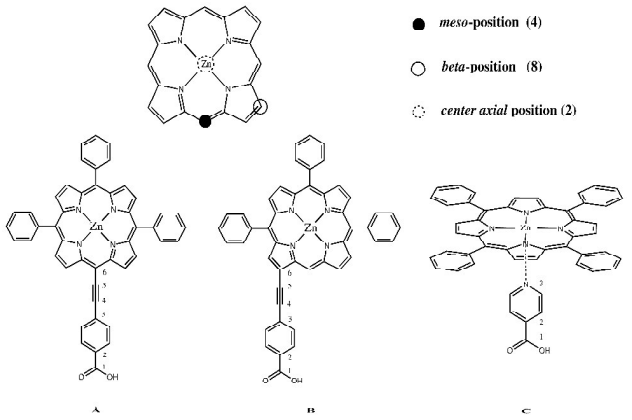

Scheme 1. Molecular structures and numbering atoms of three different Zn-porphyrin sensitizers.

2. Method

2.1 Computational details

In this work, the Gaussian09 suite of program (Revision D.01)[23] with a tight self-consistent field convergence threshold (10^{-8} au) was employed for all calculations. The DFT with the B3LYP functional[24] was used to optimize all molecules, which is a thoroughly explored method for a wide variety of dyes and dye-TiO_2 systems used in the earlier studies.[17, 25] Based on such calculations, the time-dependent density functional theory (TD-DFT)[26-28] was used to obtain the spectroscopic absorptions of three types of Zn-porphyrin sensitizers with TiO_2 model. The solvent effects of tetrahydrofuran (THF) were simulated by the polarizable continuum model (PCM).[29, 30]

In our calculations, the LanL2DZ basis sets were used to carry out the quasi-relativistic pseudopotential of Ti and Zn atoms, and the split valence basis set 6-31G(d) were employed for other atoms. The Gaussian curves were used to simulate all UV/Vis spectra under full-width at half-maximum (FWHM) of 0.10 eV. The natural bond orbital (NBO) charges analysis were performed at the same level of theory by employing the NBO 3.1 program packages under different electric field strengths. Five different electric fields of 5, 10, 15, 20 and 25 × 10^{-4} a.u. (electric field strength, 1 a.u. = 5.142 × 10^9 V/cm) paralleled to x-axis (normal to the TiO_2 surface) were applied on the isolated dye systems. As for the dye-TiO_2 systems, only two conditions are considered, without inner electric strength or with 5 × 10^{-4} a.u. inner electric strength paralleled to the x-axis.

In addition, the B3LYP functional was also selected to calculate the through-space intramolecular charge transfer (ICT). The excited-state densities have been computed within the linear-response TD-DFT framework using a vertical approximation. The electron transfer distance and the fraction of electron exchange of all sensitizers that related to the vertical transitions were calculated with Multiwfn 3.0.5. [31]

2.2 Theoretical background

As is known to all, the overall efficiency (η) of the DSSCs is defined by the ratio of the maximum output electrical power of the DSSCs to the energy of incident sunlight (P_{in}), which is determined by the short-circuit current density (J_{sc}), the open-circuit photovoltage (V_{oc}), the fill factor (*ff*) and Pin (generally AM 1.5, 100 mWcm^{-2}). The overall efficiency was calculated according to the following equation:[32]

$$\eta = \frac{J_{sc} V_{oc} ff}{P_{in}} \quad (1)$$

Short-circuit current density J_{sc}

Accordingly, the photocurrent per unit area (mAcm^{-2}) is expressed by the J_{sc} when a DSSCs under irradiation is short-circuited, which is related to the interaction between TiO_2 and dye as well as the absorption coefficient of the dye. The value of J_{sc} in DSSCs can be calculated as:[33]

$$J_{sc} = \int_{\lambda} LHE(\lambda)\phi_{inject}\eta_{collect} d\lambda \quad (2)$$

where LHE(λ) is the light harvesting efficiency at a given wavelength, Φ_{inject} denotes the electron injection efficiency, and $\eta_{collect}$ is the charge collection efficiency. First, a high J_{sc} is obtained based on equation 2, the efficient dyes used in DSSCs should have a large LHE, which is described by:

$$LHE_{\lambda} = 1 - 10^{-A} \quad (3)$$

where A is the absorption of the dye; the larger A could fulfill a better light capturing. At the same time, a large Φ_{inject} based on equation 2 could also guarantee a high J_{sc}. The Φ_{inject} is affected by the free enthalpy (ΔG) related to the electron injection from the photo-induced excited states of dyes into the TiO_2 surface. The ΔG determines the electron injection rate and can be viewed as electron injection driving force (ΔG^{inject}).[34, 35]

$$\Phi_{inject} \propto f(-\Delta G^{inject}) \quad (4)$$

$$\Delta G^{inject} = E^{dye*} - E_{CB} = E^{dye} - E_{0-0} - E_{CB} \quad (5)$$

where E^{dye*} is the oxidation potential energy of the dye in the excited state and E_{CB} is the reduction potential of TiO_2 conduction band (CB). Therefore, we used E_{CB} = -4.0 eV in this work for TiO_2 which is widely used in previous researches[15]. The E^{dye} is the oxidation potential energy of the dye in the ground state, while $E_{0\text{-}0}$ is the electronic vertical transition energy. Meanwhile, dye regeneration (ΔG^{reg}) is calculated from the difference between the ground-state oxidation potential and the redox potential of the electrolyte of electrolyte I^-/I_3^- (±4.8 eV), which is described by:

$$\Delta G^{reg} = E^{I^-/I_3^-} - E^{dye} \quad (6)$$

Open circuit photovoltage V_{OC}

V_{oc} is defined as the voltage difference between the electrolyte redox potential ($E_{redox/q}$) and the quasi-Fermi potential of electrons ($E_{F,n/q}$) in the TiO_2 semiconductor. The V_{oc} in DSSCs is expressed by:[36]

$$V_{OC} = \frac{E_{CB} + \Delta CB}{q} + \frac{k_b T}{q} \ln\left(\frac{n_c}{N_{CB}}\right) - \frac{E_{redox}}{q} \quad (7)$$

where E_{CB} is the conduction band edge of the semiconductor, E_{redox} is the electrolyte Fermi level, k_b is the Boltzmann constant, T is the absolute temperature, q is the unit charge, n_c is the number of electron in the conduction band, and N_{CB} is the accessible density of conduction band (CB) states. ΔCB is the shift of E_{CB} when the dyes are adsorbed on the semiconductor surface and can be expressed as:[33]

$$\Delta CB = -\frac{q\mu_{normal}\gamma}{\varepsilon_0 \varepsilon} \quad (8)$$

where q is the electron charge, μ_{normal} is the component of the dipole moment of the individual sensitizer perpendicular to the surface of the semiconductor, γ is the dye's surface concentration, ε is the permittivity of the dipole layer, and ε_0 is the permittivity of vacuum. It is obvious from equation 7 and 8 that a dye with large n_c and μ_{normal} would exert a crucial influence on V_{oc}.

The Stark effect is used to describe the effect of an applied electric field on an absorption or emission spectrum. The Stark spectroscopy generally represents the study of spectral changes in the presence of electric fields, which has been proven to be a wildly useful approach to characterize the changes after electron injection from excited dye sensitizer into the semiconductor electrode. Stark effects are expected to cause a small peak shift in the absorption (or emission) spectrum but no change in line shape; that is, the applied electric field, $\vec{E}$. An absorption Stark spectrum, ΔA, is the change in an absorption spectrum area under the influence of an applied electric field:[37, 38]

$$\Delta A = A(\vec{E} \neq 0) - A(\vec{E} = 0)$$

The absorption difference, ΔA, caused by the Stark effect in the spectrum of a dye-sensitized TiO_2 electrode is given by:

$$\Delta A = -\frac{dA}{d\nu} \times \frac{\Delta\vec{\mu} \times \vec{E}}{h}$$

where $dA/d\nu$ is the first derivative of the ground state dye absorption spectrum with respect to transition frequency. $\Delta\vec{\mu}$ is the change in dipole moment between ground and excited state of the dye, $\vec{E}$ is the applied electric field and h is Plank's constant.

3. Results and discussion

3.1 Molecular structure

We selected three types of Zn-porphyrin sensitizers (dye A, B and C) as models to detect the inner electric field effect on the performance of DSSCs. The structure of dye A is meso-substituted Zn-porphyrin, in which one meso position are decorated by an ethynylcarboxyphenyl group while the other three meso positions are grafted with the same phenyl groups. The structure of dye B is a β-substituted Zn-porphyrin. Compared with dye A, the only difference in this model is the substituted position of ethynylcarboxyphenyl group is changed from meso-position to the β-position. As for dye C, the structure is quite different. It can be divided into two parts of tetrakis(phenyl) Zn-porphyrin and the linker (4-pyridyl-carboxylic). The tetrakis(phenyl) Zn-porphyrin can bind to the semiconductor electrode by the linker that coordinates to the metal center in the axial position. Compared with A and B type dyes, the anchor group of C type sensitizer is obviously different, which is caused by the difference of the connection position of the anchor group to the Zn-porphyrin. We choose the 4-pyridyl- carboxylic acid as anchor group in C type dye. This anchoring group is known to bind strongly to semiconductor surfaces while the pyridyl group axially coordinates to the metal center of the Zn-porphyrin through the

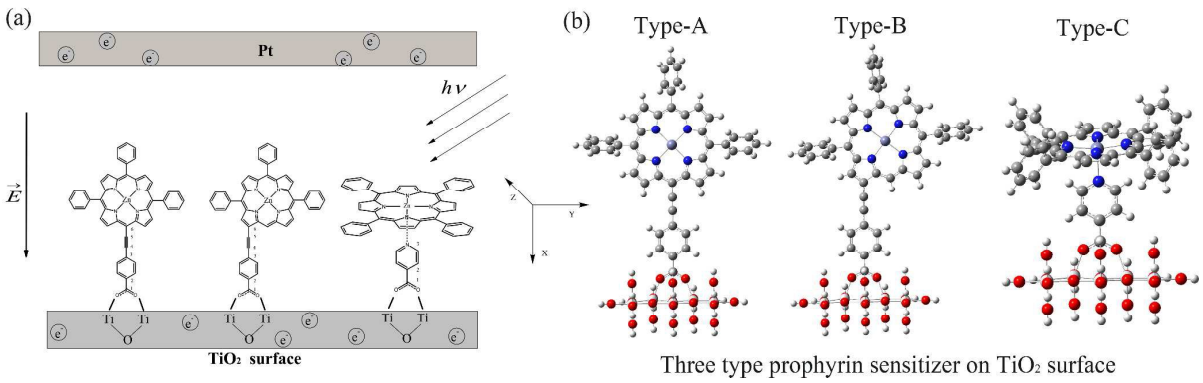

Fig. 1. (a) The direction of the inner electric field in three types Zn-porphyrin sensitizers linked on TiO_2 model system. (b) The representative geometry of three types Zn-porphyrin sensitizers linked on TiO_2 model after optimization.

pyridyl N atom, and then sensitizing the TiO_2 surface. Taking into account the representativeness and simplicity of this model, and suitable computational cost, the structures of these three types of Zn-porphyrin sensitizers were finally determined. These studied molecules can be considered as the basic structures of the different Zn-porphyrin sensitizers and their properties can reflect the real situation. In addition, three systems containing TiO_2 model and different type Zn-porphyrin sensitizers were constructed and shown in Fig. 1. In these systems, the direction from the Zn-porphyrin groups to the anchor is along with the x-axis. Considering the large size of different types of dye molecules, only the ground state structures are obtained in this work. In these three types of Zn-porphyrin sensitizers, due to the differences in geometry structure, the type C sensitizer is somewhat different from that of type A and B sensitizers. Affected by the connector group, the porphyrin macrocycle of type C sensitizer is not quite planar, but this plane was distorted a little bit. The Zn atom is out of the plane almost 9° in dihedral angle and four N atoms are almost unchanged from the planarity. Accordingly, the optimized structure was employed to calculate their electronic structures and optical properties with and without an applied electric field.

The most significant and interesting factor is the directional effect of the inner electric field. Therefore, a perfect model is needed to investigate our supposition, in which dye molecule and TiO_2 surface are ordered. The direction of the electric field is defined as the vector pointing from counter electrode to TiO_2 surface according to the electronic moving direction of inner DSSCs system, namely, the directional of the electric field is parallel to the x-axis in this work.

3.2 Absorption spectra of isolated dyes

Electronic structures are fundamental for understanding electronic absorption spectra. The schematic representation of highest occupied molecular orbitals (HOMO)-lowest unoccupied molecular orbitals (LUMO) gaps and orbital energies of selected frontier molecular orbitals (FMO) of dye A,

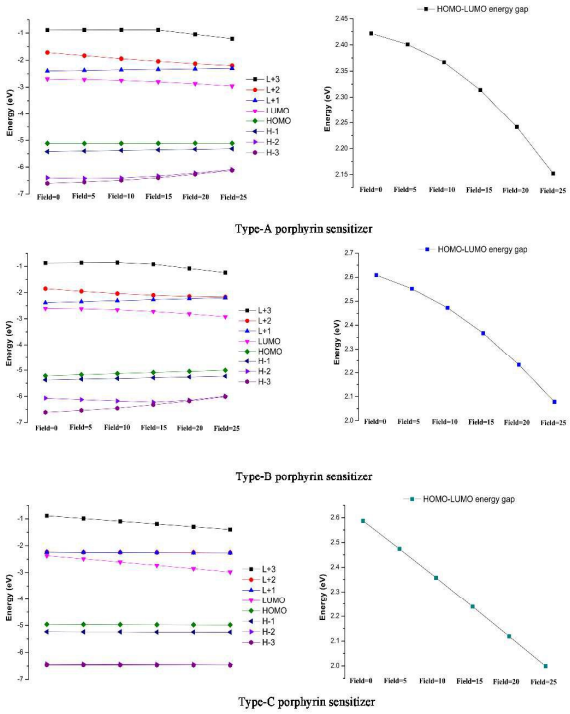

Fig. 2. The dye A, B and C system with different electric field strengths in THF solution: (left) energetic level of frontier MOs and (right) HOMO-LUMO energy gaps.

Table 1 Partial Molecular Orbital Compositions (%) of dye A system in THF solution with different electric field strengths. (The abbreviations: the Zn-Por is Zn-porphyrin, the PH is phenyl group.)

B and C under different electric field strengths are given in Fig. 2. To illuminate the effect of electric field on FMO, the LUMO and HOMO compositions of dye A system in tetrahydrofuran (THF) solution are compiled in Table 1. Besides, the important FMOs of dyes A, B and C in THF solution are displayed in Supplementary Fig. S1.

Field (10-4 a.u.)	MO	Energy(eV)	Main Component (%)				Assignment
			Zn-Por	PH	π-bridge	COOH	
Field=0	LUMO+2	-1.714	25	3	49	22	π*(Zn-phy)+*(π)+ π*(COOH)
	LUMO+1	-2.398	89	11	0	0	π*(Zn-phy)
	LUMO	-2.691	72	7	18	3	π*(Zn-phy)
	HOMO	-5.113	72	12	15	1	π*(Zn-phy)
	HOMO-1	-5.422	96	4	0	0	π(Zn-phy)
	HOMO-3	-6.605	91	9	0	0	π(Zn-phy)
Field+5	LUMO+2	-1.831	28	3	46	23	π*(Zn-phy)+π*(π)+ π*(COOH)
	LUMO+1	-2.377	89	11	0	0	π*(Zn-phy)
	LUMO	-2.714	67	6	22	5	π*(Zn-phy)+ π*(π)
	HOMO	-5.115	73	12	14	1	π(Zn-phy)
	HOMO-1	-5.400	96	4	0	0	π(Zn-phy)
	HOMO-2	-6.422	51	17	31	2	π(Zn-phy)+ π(π)
Field+10	LUMO+2	-1.943	32	3	41	23	π*(Zn-phy)+π*(π)+ π*(COOH)
	LUMO+1	-2.356	89	11	0	0	π*(Zn-phy)
	LUMO	-2.748	60	6	27	8	π*(Zn-phy)+ π*(π)
	HOMO	-5.115	73	12	13	1	π(Zn-phy)
	HOMO-1	-5.378	95	5	0	0	π(Zn-phy)
Field+15	LUMO+2	-2.044	38	4	36	22	π*(Zn-phy)+π*(π)+ π*(COOH)
	LUMO+1	-2.336	89	11	0	0	π*(Zn-phy)
	LUMO	-2.800	52	5	32	11	π*(Zn-phy)+ π*(π)
	HOMO	-5.114	73	13	13	1	π(Zn-phy)
	HOMO-1	-5.357	95	5	0	0	π(Zn-phy)
Field+20	LUMO+2	-2.129	46	4	30	20	π*(Zn-phy)+π*(π)+ π*(COOH)
	LUMO+1	-2.317	89	11	0	0	π*(Zn-phy)
	LUMO	-2.869	43	4	38	15	π*(Zn-phy)+ π*(π)
	HOMO	-5.111	73	13	12	1	π(Zn-phy)
	HOMO-1	-5.336	95	5	0	0	π(Zn-phy)
Field+25	LUMO+2	-2.198	53	5	24	18	π*(Zn-phy)+π*(π)+ π*(COOH)
	LUMO+1	-2.298	89	11	0	0	π*(Zn-phy)
	LUMO	-2.956	34	3	44	19	π*(Zn-phy)+ π*(π)
	HOMO	-5.108	72	14	12	1	π(Zn-phy)
	HOMO-1	-5.317	95	5	0	0	π(Zn-phy)
	HOMO-4	-6.398	91	9	0	0	π(Zn-phy)

For the studied dye A, the occupied molecular orbitals of these systems can be labeled as π (Zn-por) orbitals in character, but substantially mixed with the π (PH) character. And the unoccupied molecular orbitals of dye A under different electric field strengths can be labeled as π* orbitals of Zn-porphyrin and π-bridge in character. Taking into account different electric field strengths, the change of energy levels for HOMO are not obvious while for LUMO are gradually decreased. Therefore, the HOMO-LUMO energy gaps of dye A under different electric fields are smaller than that of the dye without electric field. In general, the number of occupied MOs and unoccupied MOs involved in absorption transition process is qualitatively similar. However, when an electric field is applied on the dye of this type, it will significantly affect the energy of occupied molecular orbitals whereas the influence on the energy of unoccupied molecular orbitals is slight.

There are eight frontier molecular orbitals (four occupied MOs and four unoccupied MOs) for dye A system as shown in Fig. 2. The distribution of energy levels and the changing trend of the frontier molecular orbitals can be clearly observed from this figure. Considering the changing trend, the HOMO, H-1 and L+1 are not influenced with the energy that unchanged basically under the applied electric fields. For LUMO, L+2 and L+3, the orbital energy is gradually reduced along with the increasing electric field strength. As for H-2 and H-3, the overall trend is that their energies gradually increase along with the increasing electric field strength.

Based on the above results, the frontier molecular orbitals of dye A are obviously influenced by the inner electric field. There are some similar varying tendencies in dye A under

different electric field strengths. Firstly, the variation tendency of part of LUMOs under different electric field is from π* (Zn-por) and π* (PH) to π* (π-bridge) and π* (COOH), respectively. Namely, the component of π-bridge is gradually increased while the components of Zn-porphyrin and phenyl groups are gradually decreased with the increase of electric field intensity. Meanwhile, the six LUMOs of dye A under different electric field strengths are composed of π* orbitals localized on the Zn-porphyrin and partly on the π-bridge. Especially, it is found that more orbital contribution is derived from the carboxylic groups with the increase of electric field. This is advantageous for larger charge collection efficiency. The transferred electron can reach the conduction band of the semi-conductor via photo (sunlight) excitation since the sensitizer can interact with the semi-conductor via the carboxyl group. Secondly, the energies and ingredients of HOMOs under different electric fields are almost constant. In other words, the HOMOs of dye A with or without inner electric field are quite stable. Furthermore, the inner electric field effect on the HOMO-LUMO energy gap was also investigated by using different electric field intensity. Obviously, the HOMO-LUMO gaps of the dye A under an electric field are smaller than those of the one without applying an electric field. The HOMO-LUMO energy gaps of all dye A systems decrease in the order of 2.422 eV (field=0) > 2.401 eV (field=5) > 2.367 eV (field=10) > 2.314 eV (field=15) > 2.242 eV (field=20) > 2.152 eV (field=25). The result demonstrates that the absorption spectra are systematically red-shifted with the increasing electric field. These properties could be in favor of abundant absorption in long-wavelength region.

In comparison to dye A, the variation tendency of dye B systems (see Supplementary Table S1) is similar but with some difference in that of the HOMO energy. The varying tendency of the energy of HOMOs under different electric field is gradually increased, while the components of HOMOs have changed little. Therefore, the HOMO-LUMO energy gaps of all dye B systems decrease in the order of system 2.609 eV (field=0) > 2.552 eV (field=5) > 2.473 eV (field=10) > 2.367 eV (field=15) > 2.233 eV (field=20) > 2.078 eV (field=25).

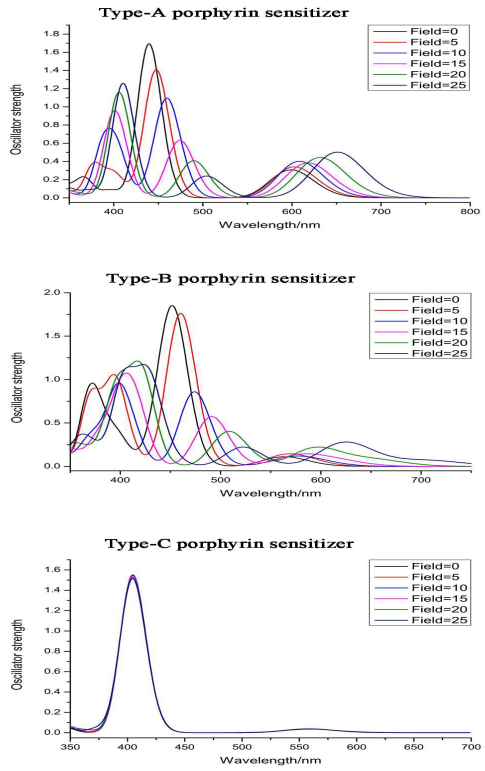

Fig. 3. Simulated absorption spectra of dye A, B and C systems under different field strengths in THF solution.

Interestingly, unlike dye A and B systems, there are four degenerate orbitals in FMOs of dye C system (see Supplementary Table S2). It is obvious that the LUMO+1 and the LUMO+2 of dye C are mainly delocalized on the Zn-porphyrin ring and phenyl groups. The energies of LUMO+1 and the LUMO+2 nearly degenerate with a difference of 0.001-0.007 eV under different electric fields，and the ingredients are the same. Besides, for occupied MOs, the HOMO-2 and HOMO-3 also degenerate. Overall, the all occupied molecular orbitals and L+1 and LUMO+2 are not influenced with the energy that unchanged basically under the applied electric fields.

For LUMO and L+3, the orbital energies decrease progressively with the increasing electric field strength. Finally, the energy gaps of HOMO-LUMO for all dye C systems decrease in the order of 2.587 eV (field=0) > 2.474 eV (field=5) > 2.358 eV (field=10) > 2.239 eV (field=15) > 2.119 eV (field=20) > 1.999 eV (field=25).

The absorption spectra of dyes A, B and C in the THF solution were also obtained by employing the TD-B3LYP method to reveal the solvent effect on the optical properties. The absorption results of dye A systems associated with its oscillator strengths and main excitation are summarized in Table S3. The fitted Gaussian-type absorption curves between 350–750 nm based on the calculated absorption data are shown in Fig. 3.

Taking dye A as an example, two strong absorption bands were obtained with the absorption peaks at 599 and 441 nm without inducing electric field. It can be clearly seen that the absorption spectra can be divided into two main regions with the first intense peak in the 400-500 nm region and the second peak in the range of 550-650 nm. The excitation of H-1→L+1 and HOMO→L+2 contributed to the strongest absorption at 441 nm while the second strong absorption at 599 nm mainly proceeds through HOMO-LUMO. These main electron transitions can be assigned to the intra Zn-porphyrin charge transfer.

The absorption spectra of dye A with different electric field were simulated for the insight of the optical property and electronic transition. The simulated absorption spectra of dye A under different electric fields reveal that the lowest-energy absorption (λ_{max}) bands red shift from 599 to 651 with the enhancement of the electric field strengths from 0 to 25 $\times 10^{-4}$ a.u. The results indicate that the electron transitions for the lowest-energy absorption bands mainly originate from the HOMO→LUMO transition. Meanwhile, the oscillator strengths of the lowest-energy absorption peaks of dyes with different electric field strengths are higher than that without electric field. The reason is that the distribution of electron cloud involved in orbital could be affected by the electric field, which contributes to a higher overlap during electron transitions. Clearly, the changes of these spectra could be ascribed to the inner electric field. Therefore, these absorptions are beneficial to the light harvesting efficiency and thus affecting the performance of DSSCs.

For all the dye B systems (see Supplementary Table S4), there are three absorption bands in dye B without electric field. The strongest absorption at 453 nm is contributed by excitation HOMO→L+1 and H-1→LUMO. This is this excitation can be assigned as intra Zn-porphyrin charge transfer. In addition, the excitations responsible for the other strong absorption at 367 nm originate from H-1 to L+2. This excitation can be ascribed as π (Zn-phy) and π (π-bridge) to π* (Zn-phy) and π* (π-bridge) transition character and the COOH groups taking part in the transition process. The excitations of HOMO→LUMO and H-1→L+1 excitation leads to the lowest energy absorption at 570 nm, which can also be assigned as intra Zn-porphyrin charge transfer. Moreover, the lowest-energy absorption (λ_{max}) bands of the dye B red shift from 570 to 706 nm with the enhancement of electric field strengths from 0 to 25 $\times$ 10^{-4} au. On the whole, the change trend of the absorption is the same as that of the dye A system, so we think indicating that the effect of the inner electric field is the same as that of the dye A system.

Moreover, different from the dye A and B systems, the dye C system (see Supplementary Table S5) has simple absorption properties without electric field. The strongest peak at 404 nm is contributed by excitation H-1→L+1 and HOMO→L+2. This absorption peak could be assigned as the electron transfer from the contribution of π orbitals of Zn-porphyrin to π* orbitals of Zn-porphyrin itself. For the other absorption peak at 451 nm, the excitation of HOMO→L+2 and H-1→L+1 are in charge of it and can be also assigned as intra Zn-porphyrin. The calculated lowest energy absorption with very weak oscillator strength (0.0058, the weakest among the calculated absorptions) at 595 nm is contributed by HOMO→LUMO excitation. This electron transitions can be assigned to the charge transfer from the Zn-porphyrin to the π-conjugation bridge and COOH group. The changes of electric field have little effect on the absorption spectrum of dye C systems. Although the lowest-energy absorption bands red shift from 595 to 826 nm along with the increasing electric field strength, their oscillator strengths are so weak that they can be ignored. For other two strong absorption peaks, the oscillator strength and position are the same, and no change has occurred.

To summarize, the calculated UV-visible absorptions of all three type dyes are influenced by the inner electric field except for dye C systems. The absorption spectra of dye A and B systems are gradually broadened and red-shifted while the increase of electric field strength. Therefore, these absorptions are helpful for charge transfer in DSSC.

3.3 Absorption spectra of three types of sensitizers on TiO_2 surface

As a matter of fact, dye sensitizers are mainly connected onto the surface of nanometer-size TiO_2 in a DSSC. The adsorption model of dye attached on TiO_2 is important to the electron injection process. Hence, it is worth pointing out that calculations for the properties of the dye-adsorbed TiO_2 systems.

The choice of the TiO_2 model in our simulation is vital for the rationality and accuracy. In general, anatase nano-TiO_2 form is more photo-catalytic than that the rutile, and nanoscale rutile less photo-reactive than anatase. Moreover, titanium dioxide (101) surfaces, most thermodynamically stable in nano-crystal, dominated the majority of the external surface of TiO_2 (more than 94% percent).[39] Actually, the large models of TiO_2 are likely to represent the real TiO_2 surface while the advisable approximation of adopted model is necessary. The effect of orbital coupling is considered before designing the final ideal model. Those Ti atoms connected directly with carboxyl group should make an overwhelming contribution to the charge-transfer process, which afford primary transition-related orbitals in the absorption process. And it could be concluded that the distance between Ti atoms and the anchoring group become key factors. Take into account the computational cost and size, finally, anatase $Ti_5O_{20}H_{22}$ (101) model from crystal structures was adopted as the surface of TiO_2 film in the current work.[17, 40] This model is cut out from the relaxed surface slab. These Ti atoms can be divided into two types: one is five-coordinated and the other is six-coordinated. The five-coordinated Ti atoms are located at anatase (101) surface, which used for adsorption site. In addition, the six-coordinated Ti atoms are cut out from the TiO_2 crystal bulk. Hydrogen saturators were used on oxygen atoms, and this method not only maintains bond-orientation in crystal, but also avoids the chaos of charge and multiplicity in the whole system.

Besides, the electronic structure of the TiO_2 model was analyzed. The density of states (DOS) is presented in Supplementary Fig. S2. Moreover, to illustrate the electronic structure, the frontier molecular orbital compositions are listed

in following Table S6. These characters are in accordance with that of the understanding in TiO_2 semiconductor material.

Table 2 Partial Molecular Orbital Compositions (%) of dye A absorb on TiO_2 in THF solution with different electric field strengths

Dye	Field (10-4 a.u.)	MO	Energy (eV)	Main Component (%)		Assignment
				dye	TiO_2	
A	0	LUMO+14	-2.361	1	99	d (TiO_2)
		LUMO+13	-2.422	81	19	π* (dye)+d (TiO_2)
		LUMO+11	-2.587		100	d (TiO_2)
		LUMO+10	-2.600	3	97	d (TiO_2)
		LUMO+4	-3.119	16	84	d (TiO_2)+ π* (dye)
		LUMO+2	-3.332	5	95	d (TiO2)
		LUMO+1	-3.366	21	79	d (TiO_2)+ π* (dye)
		LUMO	-3.609	9	91	d (TiO_2)
		HOMO	-5.350	100		π (dye)
		HOMO-1	-5.621	100		π (dye)
		HOMO-2	-6.661	100		π (dye)
		HOMO-6	-6.942	100		π (dye)
	5	LUMO+15	-2.478	85	15	π* (dye)+d (TiO_2)
		LUMO+14	-2.522	100		π* (dye)
		LUMO+6	-3.128	33	67	d (TiO_2)+ π* (dye)
		LUMO+4	-3.375	5	95	d (TiO_2)
		LUMO+3	-3.450	6	94	d (TiO_2)
		LUMO+2	-3.589	8	92	d (TiO_2)
		LUMO+1	-3.619	6	94	d (TiO_2)
		LUMO	-3.866	6	94	d (TiO_2)
		HOMO	-5.312	100		π (dye)
		HOMO-1	-5.554	100		π (dye)
		HOMO-2	-6.611	100		π (dye)
		HOMO-4	-6.788	100		π (dye)

Compared with the conduction band edge position of -4.3 eV for anatase, the LUMO energy level of single-crystal anatase $(TiO_2)_5$ model (location at -4.281 eV) has provided the more approximate and corresponding result. Thereby, the electronic structure and related results of the single-crystal anatase $(TiO_2)_5$ model are reasonable and accurate for describing the conduction band properties of the semiconductor.

In DSSCs device, besides the neutral forms, the dye sensitizers will dissociate and adsorb on the semiconductor surface. Following this, we investigate the connection type between dye molecules and TiO_2 film. Essentially, the carboxylic acid groups as the linker which ensuring efficient adsorption of the dye on the surface and also promoting electronic coupling between the donor of the excited dye sensitizer and the favorable acceptor levels of the TiO_2 semiconductor. The type of anchor functionality and linker between the sensitizer and semiconductor surface can enhance electronic coupling and/or alter the surface state energetic activity, so that electron injection is faster and more efficient. Consequentially, the connection type between dye molecules and the TiO_2 film is a crucial factor for electron injection process.[41] At last the bidentate bridging type is appropriate in this work. The bidentate bridging type is firm, which is the most important connection type causing the interaction strength and absorption efficiency in our systems. According to the calculation, the bond lengths between two carboxylate oxygens and connected titanium atoms on the TiO_2 model of the dye A, B and C systems are 2.053/2.130 Å, 2.061/2.133 Å and 2.085/2.180 Å, respectively. Compared to the bond length data of TiO_2 film (1.930 and 1.973 Å) and calculated data, our data has provided more approximate result. In this contribution, the bidentate bridging type is considered throughout for reasonable connection mode and for suitable distance within the binding.

In the same way, the approximate dye-TiO_2 structure was employed to calculate the electronic structures and optical properties with and without an applied electric field. The frontier molecular orbitals which responsible for absorption wavelength (λ) longer than 350 nm (see Fig. 4), are plotted according to their energies. Furthermore, orbital compositions of A-TiO_2 systems are summarized in Table 2. In this work, the orbital-coupling is an effective way of orbital overlap to reduce the orbital energy, which is done by combining the p orbital of

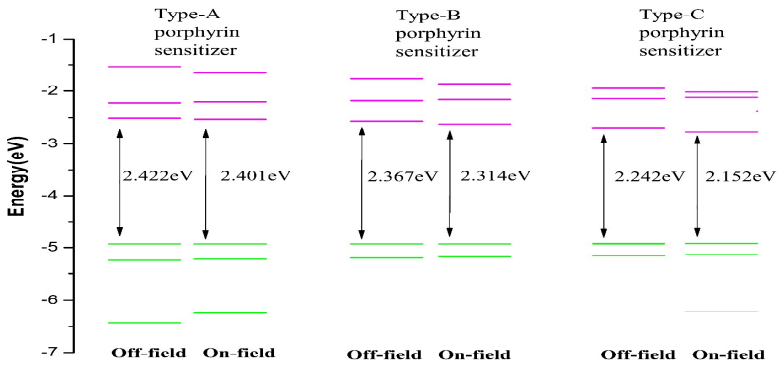

Fig. 4. The plot of the frontier MOs relevant to the absorptions for dye A, B and C absorbed on TiO_2 model with and without electric field strength in THF solution.

the carboxyl group with the d orbital of TiO_2 semiconductor to extend the π-conjugate degree and increase the charge injection ability. The interaction between dye sensitizer and TiO_2 semiconductor is present in the dye-TiO_2 system and it is hard to analyze separately the character of dye and TiO_2 semiconductor as the dye and TiO_2 semiconductor are considered completely a unitary system. Although the orbitals couple cannot be expressed with clear numerical form, it can determine the strength of the orbitals couple by the energy and the contribution ratio of the main component. So, we think that it is still significant to study the dye-TiO_2 system in this way. Molecular orbital profiles of frontier molecular orbitals, involved in lowest-energy absorption, are shown in Supplementary Fig. S3, illustrating the charge injection from dye molecules into the conduction band of the TiO_2 film.

For A-TiO_2 systems, similar to the isolated dye A, the change of HOMO energy levels is not obvious, but the LUMO energy levels are gradually decreased with increasing electric field strength. Herein, the HOMO-LUMO energy gap of the A-TiO_2 systems without electric field (2.422 eV) is larger than that of A-TiO_2 systems with electric field (2.401 eV). Due to the similar properties of occupied molecular orbital for A-TiO_2 systems with and without electric field strength, for which the HOMO entirely lies on the dye A, we only need to pay attention to the unoccupied molecular orbital. In the condition without electric field, orbital-coupling is well between the dye and TiO_2 semiconductor so that, can reduce the orbital energy level. The LUMO is mainly composed of the TiO_2 film with compositions up to 91%. The high photo-voltaic converting efficiency of DSSCs requires rapid and efficient electron injection from the excited state of dye into conduction bond of TiO_2 film. Thus, when absorption happens, we believe that the electrons were stimulated and entered in to TiO_2 film directly.

However, it is surprising that the situation has changed as applying the inner electric field. The energies of the LUMOs decline obviously leading to the main components of the LUMOs from dye molecule into TiO_2 film. In other words, because of the change in field strength, the proportion of TiO_2 film increases and the proportion of dye A decreases in the LUMO composition. Similar to the field=0 condition, electrons injection ultrafast excited-state electron injection is the primary way of charge transfer from dye A to TiO_2 film. Moreover, it would result in long-time scale and high utilization of solar.

When the dye B and C molecules (see Supplementary Table S7 and Table S8) are connected to TiO_2 film in (101) surface, the effects of the applied electric field on them are the same as those of the A-TiO_2 system. The HOMO-LUMO energy gaps of the dye B and C on TiO_2 surface systems both decrease in the order of 2.367 eV (off-field) > 2.314 eV (on-field) and 2.242 eV (off-field) > 2.152 eV (on-field). Meanwhile，the main components of the LUMOs are from dye molecule into TiO_2 film for B-TiO_2 and C-TiO_2 systems. Generally, the inner electric field could deeply affect the distribution of energy levels and components of the frontier molecular orbitals, and the influence on the spectrum needs further analysis.

In addition, the fitted Gaussian-type absorption curves based on the calculated absorption data are shown in Fig. 5. For A-TiO_2 system, all dominant excitations in the absorption process are listed in Table S9. We seek to understand the effect of the inner electric field on absorption behavior of different type sensitizers, and its impact on the efficiency of different type sensitizers is demonstrated in this paper. Five strong absorption bands were calculated with the absorption peaks at 405, 486, 630, 715 and 830 nm for A-TiO_2 system without electric field. The strongest absorption at 405 nm, the excitation responsible for it originate from in the same the occupied orbital H-1 but terminate different virtual orbital L+13 and L+14. Although the number of absorption bands is very large and the orbitals involved in the transition process are very complex, the nature of the transition can be divided into two categories. One category is assigned as the electron transfer completely from the contribution of the π orbitals of dye molecule to d orbitals of TiO_2, such as absorption bands at 830 nm. The other is assigned as the electron transfer from the contribution of the π orbitals of dye molecule to d orbitals of TiO_2 and the π orbitals of dye molecule partially taking part in the transition process, such as absorption bands at 405, 486, 630 and 715 nm. These facts showed a satisfactory electronic coupling between dye and the semiconductor surface with enforced the direct electron transfer mechanism.

The absorption of dye A-TiO_2 system under electric field is quite different with that from the off-field system, especially for the oscillator strength and absorption range. The absorption spectra of A-TiO_2 system with electric field present the lowest energy absorption peak at 1033 nm, which is clearly shifted to longer wavelengths relative to that of the off-field condition. Moreover, the strongest absorption wavelength of the A-TiO_2 with electric field system is at 410 nm, and the electric field has little effect on the strongest absorption position but has an enhanced effect obviously on the oscillator strength. This transitions composition of dye molecule itself is increased for the strongest absorption composition, but the proportion of this contribution is not large (29%). The main transition process is still the charge transfer from the dye molecule to the semiconductor, thus this transition is conducive to electron injection.

There are three strong absorption peaks in the B-TiO_2 system. The strongest absorption at 401 nm is contributed by excitation H-1→L+11 and HOMO→L+13 (see Supplementary Table S10). The calculated lowest energy absorption at 802 nm cannot be distinguished in the absorption spectrum, this may be due to its weak oscillator strength (0.0160, the weakest among the calculated absorptions). The characters of the transition are essentially the same as that of the A-TiO_2 system, thus so it has a similar electron injection mechanism.

For dye B-TiO_2 system under electric field system, the absorption becomes red-shift due to the existence of the electric field. In addition, the oscillator strengths of absorption peaks become smaller than that off-field condition. The lowest energy absorption peak is shifted to longer wavelengths at 1025 nm. More importantly, the strongest absorption at 406 nm, the biggest difference rests with the increase of the dye molecule itself transition contribution. It is contributed by H-1→L+15 and HOMO→L+14 excitation, and this excitation can be ascribed to the charge transfer of dye molecules itself. This kind of charge-transfer would lead to emission or relaxation oscillation electron injection, namely, dye B is excited from the ground states and then the excited electron is injected into the CB of the semiconductor, which would result in long-time scale and low utilization of solar.

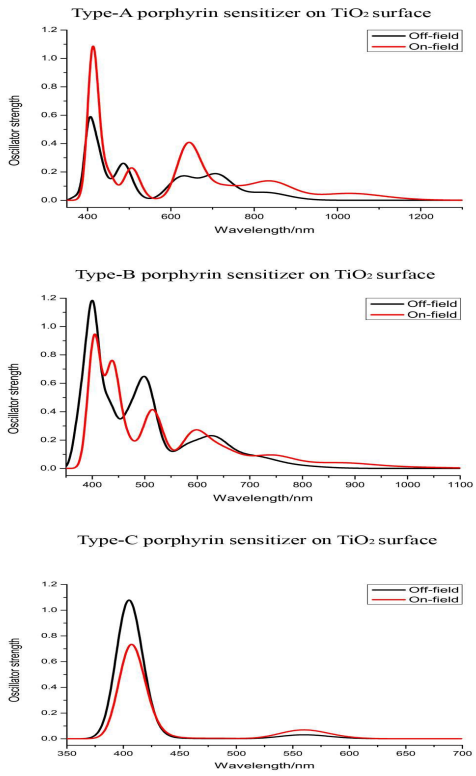

Fig. 5. Simulated absorption spectra of dye A, B and C on TiO_2 model with and without electric field strengths in THF solution.

As for the C-TiO_2 system, its absorption curve is very simple (see Supplementary Table S11). As can be seen that there are only two absorption peaks for this system, in which the strongest absorption at 311 nm is contributed by excitation H-1→L+14 and HOMO→L+15, whereas the excitations of HOMO→L+15 and H-1→L+14 lead to lowest energy absorption at 560 nm. All excitations can be ascribed to dye molecules itself charge transfer.

While the C-TiO_2 system with electric field, the absorption spectrum is almost the same as that of the C-TiO_2 system without electric field, but the oscillator strength is low. From the nature of the transition point of view, the properties are similar to C-TiO_2 system without electric field. The biggest difference is that there is a transition from the dye C to the TiO_2 model charge transfer. However, the proportion of this contribution is not large, the dye molecule itself charge transfer still is the main transition. Hence, the inner electric field has no obvious effect on the absorption of C system.

To summarize, the transition from HOMO with dye orbital character to LUMO with prominent TiO_2 will shift to lower energy side with the present of the inner electric field. Then, we can easily understand the new peaks and intensity changes of absorptions. Moreover, it is found that the inner electric field has different effects on the absorption spectra of different Zn-porphyrin sensitizers. Therefore, the inner electric field is an

important influencing factor for the best performance of the dye sensitizers.

3.4 Intramolecular charge transfer

Effective electron-hole separation of dye sensitizer is a crucial factor to obtain high photocurrent conversion efficiency. It originated from the intramolecular electronic excitation to a charge transfer state upon photo-excitation. Especially for the structure of Push−Pull Zinc Porphyrin sensitizers, scientific workers have done in-depth research recently.[42-44] These studies have pointed out that the insertion of an electron donating group at the proper position is useful methods to improve the efficiency of the DSSCs. Meanwhile, we believe that the model of all three types of sensitizer also has the push-pull function. In this work, the Zn-porphyrin is considered to be a donor. Generally, the Zn-porphyrin is connected to one more electron donor group for the real sensitizers, in order to achieve the purpose of enhancing the electron-donating ability. Secondly, the anchor carboxyl group of the sensitizers is used as as acceptor. Finally, the structure between the porphyrin and the carboxyl group is also the π-bridge. In our view, the results of type A sensitizer are also applicable to the push-pull type molecules. Therefore, towards an understanding of the processes of different type Push−Pull Zinc Porphyrin sensitizers involved in the intramolecular electron transfer under different inner electric field are very important for DSSCs.

Ciofini et al. put forward a simple and effective dipolar approach to quantify charge transfer phenomena.[45] And, this method was successfully used to study every electron transition of various types of dye molecules, such as Ru-based complexes, organic sensitizer and Zn-porphyrin sensitizer.[46-48] The electronic densities derived from the ground and excited states for their vertical electronic excitation (ρ_{GS}(r) and ρ_{EX}(r), respectively) were defined. Subsequently, two functions ρ+(r) and ρ-(r) can be given to defining the increase and decrease of the density owing to the electron transition. The barycenters of the spatial regions defined by ρ+(r) and ρ-(r), can be written as:

$$R_+ = \frac{\int r\rho_+(r)dr}{\int \rho_+(r)dr} = (x_+, y_+, z_+)$$

$$R_- = \frac{\int r\rho_-(r)dr}{\int \rho_-(r)dr} = (x_-, y_-, z_-)$$

The distance of charge transfer (D_{CT}) can be defined as:

$$D_{CT} = \left|R_+ - R_-\right|$$

Integrating over all the space ρ+(r) (or ρ-(r)), the transferred charge (q_{CT}) can be defined. Analogously, the dipole moment variation between the ground and the excited states (μ_{CT}) can be computed by the following relations:

$$\left\|\mu_{CT}\right\| = d_{CT}\int \rho_+(r)dr = -d_{CT}\int \rho_-(r)dr = D_{CT}q_{CT}$$

For visualization purpose, two intuitive anisotropic Gaussian distributions of charge associated with the positive and negative density regions are defined as follows. The root-mean-square deviations which represent the distributions of density variation along the three axes ($\sigma_{a,j}$, j=x, y, z; a= + or -) are computed as:

$$\sigma_{a,j} = \sqrt{\Sigma_i \rho_a(r_i)(j_i - j_a)^2 / \Sigma_i \rho_a(r_i)}$$

Then, two anisotropic Gaussian distributions (C_a, a= + or -) are simply defined as:

$$C_a(r) = A_a \exp\left(\Sigma_{j=x,y,z} -(j - j_a)^2 / 2\sigma_{a,j}^2\right)$$

where A_a (a= + or -) are the normalization factors. The index H, the half of the sum of the Gaussian distribution axis along the D-A direction has been computed. For example, if the inner electric field direction is along the x axis, H is defined as:

$$H = \frac{\sigma_{+x} + \sigma_{-x}}{2}$$

The t represents the difference between DCT and H:

$$t = D_{ct} - H$$

t, which is a tool that can be used to define the degree of through space character of an electronic transition.

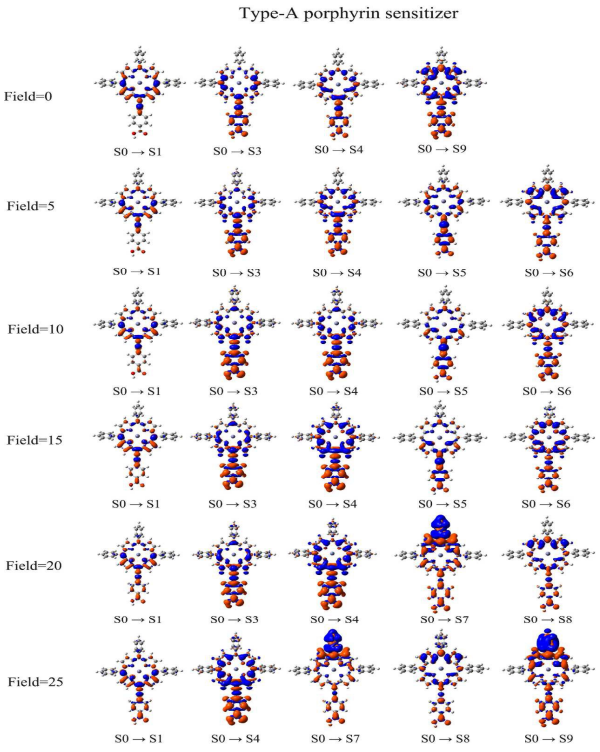

Fig. 6. Computed electronic density variation Δρ for selected transitions of dye A system with different electric field strengths. The blue and orange lobes represent a density increase and depletion upon excitation, respectively.

Table 3 The main parameters r of the dye A with different electric field strengths for the charge transfer under B3LYP/6-31G(d) level in THF

Field (10^{-4} a.u.)	NO.	D_{CT} (Å)	q_{CT} (e)	μ_{CT} (Debye)	H(Å)	t(Å)	$Overlap_{C+C-}$
0	1	0.610	0.213	0.623	4.890	-4.280	0.968
	3	3.629	0.353	6.158	5.467	-1.838	0.918
	4	3.389	0.316	5.141	5.407	-5.091	0.924
	9	4.030	0.519	10.038	5.680	-1.650	0.863
5	1	1.099	0.223	1.174	5.002	-3.903	0.953
	3	4.413	0.449	9.507	5.367	-0.954	0.862
	4	4.296	0.421	8.694	5.421	-1.125	0.875
	5	1.576	0.315	2.383	5.631	-4.055	0.969
	6	3.586	0.369	6.356	5.734	-2.148	0.905
10	1	1.604	0.237	1.829	5.124	-3.520	0.939
	3	4.733	0.518	11.769	5.315	-0.582	0.829
	4	4.669	0.539	12.077	5.409	-0.740	0.849
	5	1.418	0.273	1.856	5.508	-4.090	0.979
	6	3.655	0.413	7.246	5.728	-2.073	0.897
15	1	2.125	0.258	2.629	5.214	-3.089	0.925
	3	4.830	0.555	12.881	5.305	-0.475	0.816
	4	4.800	0.630	14.518	5.409	-0.609	0.840
	5	1.548	0.254	1.548	5.479	-3.931	0.984
	6	3.630	0.393	6.847	5.799	-2.169	0.904
20	1	2.651	0.284	3.615	5.346	-2.695	0.911
	3	4.852	0.560	13.048	5.320	-0.468	0.813
	4	4.814	0.674	15.585	5.416	-0.602	0.839
	7	4.765	0.747	17.108	5.471	-0.706	0.821
	8	3.688	0.322	5.705	5.789	-2.101	0.895
25	1	3.152	0.318	3.152	5.435	-2.283	0.897
	4	4.775	0.664	15.238	5.433	-0.658	0.843
	7	4.749	0.606	13.821	5.632	-0.883	0.830
	8	3.995	0.314	6.029	5.889	-1.894	0.898
	9	5.111	0.747	5.111	5.817	-0.706	0.835

Finally, the overlapping extent between C_+ (r) and C_- (r) is used to evaluate the charge separation degree. It is defined as:

$$Overlap_{C+C-} = \int \sqrt{C_+(r)/A_+}\sqrt{C_-(r)/A_-}\,dr$$

The value near to 1 means that the two functions are completely overlapped, and it approaches 0 indicating that they are completely separated.

In order to analyze the nature of the electronic transitions responsible for the absorption spectrum of three type Zn-porphyrin sensitizer, the key parameters and the associated indexes of dye A systems are calculated and the results are presented in Table 3. The electron density difference plots gave a clear vision of electron movement after photo-excitation. The relevant difference density plots of dye A systems are collected in Fig. 6. Our purpose is to illustrate how the inner electric field affects the charge separation and the electron transfer process of three type Zn-porphyrin sensitizers, which is important for understanding the different photo-to-electric efficiency of different type Zn-porphyrin sensitizerIn the first instance, the porphyrin ring has generally a donor behavior for dye A without electric field system except in the case of the 1st transition. They show the donor character towards the ethynylbenzoic acid carrying the anchoring group and thus expected to be particularly efficient for charge injection. The Zn-porphyrin actually plays the role of a primary donor group and it is found to be involved in the 3rd, 4th, and 9th transitions all of the charge transfer characters.

This analysis is numerically quantified by the inspection of the computed associated D_{CT} values which are of 3.629, 3.389 and 4.030 Å for the 3rd, 4th and 9th, respectively, and only of 0.610 Å for the first transition. Fortunately, this transition is also the relatively weak so the light is expected to be mainly absorbed by efficient transitions for charge injection that is those that bring the electron density closer to the COOH group. Moreover, the q_{CT} values of the 3rd, 4th and 9th are 0.353, 0.316 and 0.519 e, respectively, which are much larger than that of 1st (0.213 e). That is, the most efficient transitions for charge injection seem to be the 3rd, 4th and 9th transitions since they combine important q_{CT} values to a strong increase in the electronic density of the anchoring group that could lead to

quick electron injection by enhancing the electronic coupling between the sensitizer and the semiconductor surface.

Different from dye A without electric field system, the transitions of dye B with electric field systems (see Supplementary Fig. S4 and Table S12) are not only in the number of major transitions but also in nature. With the enhancement of the electric field strength, the number of the main transition increases. Meanwhile, D_{CT} and q_{CT} values gradually become larger with the increase of the electric field strength. The $Overlap_{C+-C-}$ values for dye B with electric field systems generally become smaller which indicates the degree of electron-hole separation become larger as the electric field strength increases. All transitions show similar properties, namely, the charge transfers from Zn-porphyrin to anchoring group. Thus, the inner electric field has a positive effect on the dye A system.

For the sake of simplicity clarity only change trends of dye B system with and without electric field will be discussed. The porphyrin ring has both donor and acceptor behavior for dye B without electric field system. This shows that β-substituded may not be as good as meso-substituted porphyrin sensitizer. However, the situation is changed when the inner electric field present. D_{CT} and q_{CT} values gradually become larger with the increase of the electric field strength. In addition, due to the $Overlap_{C+-C-}$ values for dye B with electric field systems generally become smaller, electron-hole separation become larger. Importantly, the nature of all transitions has changed; the porphyrin ring has completely donor properties so that the charge transfers become form Zn-porphyrin and phenyl groups to anchoring group. In the same way, the inner electric field has a positive effect on the dye B system.

Interestingly, and contrary to what discussed in the cases of dye A and B under different electric field systems, the transitions of dye C systems (see Supplementary Fig. S5 and Table S13) under different electric field systems are essentially the same. That is, the inner electric field has little effect on the dye C system. On the whole, no matter how the electric field strength is changed, the porphyrin ring always behaves as both donor and acceptor for dye C system. Therefore, compared to the two systems above, electron injection of dye C system will slow down, which may also be a factor in the low efficiency of C type Zn-porphyrin sensitizer.

3.5 Electrostatic potentials and natural bond orbital analysis

We focused on the relationship between the inner electric field and the charge distribution properties. The electrostatic potential (EPS) map can be considered as an indicator of charge distribution. As can be seen from Fig. 7, for the off-field condition, the negative charges are located on tetrapyrrole macrocycle and the O atom of the carboxyl group for the dye A and B systems. Meanwhile, the positive charges are mainly located on Zn^{2+} cation, phenyl groups and the H atom of the carboxyl group. It is well known that an efficient sensitizer used in DSSC is normally featured with a donor-π-acceptor (D-π-A) structure. Herein, the Zn-porphyrin core is considered as a donor group, and the electron-donating group such as phenyl groups attached to the Zn-porphyrin can enhance the donating electron capability of the donor group, raising the possibility of accepting electrons by the π-bridge and anchoring group. This also has a positive effect on the performance of the obtained DSSCs.

Conversely, we can find obvious differences among the distributions of ESP for dye A and B systems under different electric field strengths. Under the electric field, the negative charge region is still partly located on tetrapyrrole macrocycle of dye A and B sensitizer, but the negative charge region becomes smaller with the increasing field strength. Moreover, the positive charge region for the phenyl groups gradually

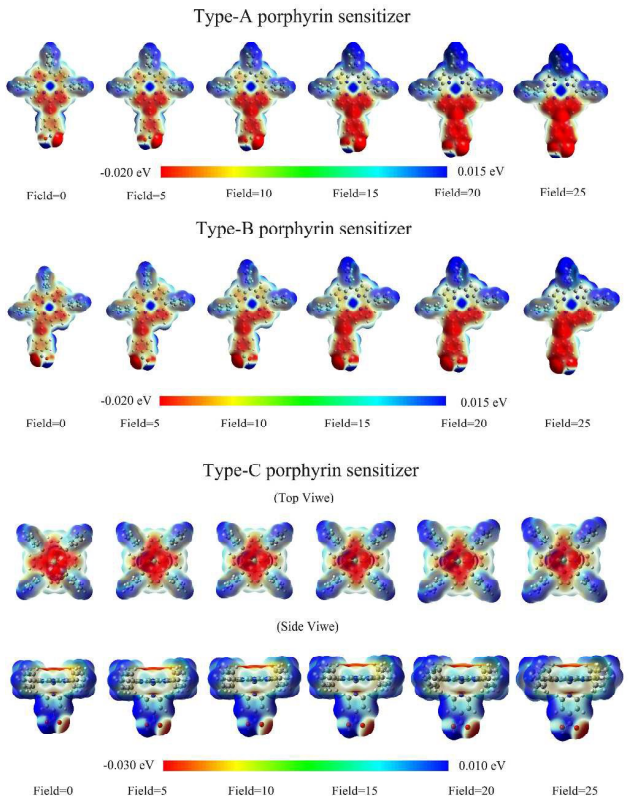

Fig. 7. Maps of electrostatic potential for dye A, B and C with different electric field strengths. (Blue and red represents positive and negative, respectively.)

Table 4 Effects of electric field on the natural bond orbitals (NBOs) charge for the dye A with different electric field strengths.

Field (10^{-4} a.u.)	Natural bond orbital (NBO) charge (e)						$\mu_{x\text{-bare}}$ (Debye)
	C_1	C_2	C_3	C_4	C_5	C_6	
Field=0	0.766	-0.168	-0.092	-0.001	0.021	-0.112	-5.1421
Field=5	0.766	-0.172	-0.089	-0.008	0.027	-0.116	-7.3393
Field=10	0.766	-0.175	-0.086	-0.014	0.032	-0.120	-9.5785
Field=15	0.766	-0.179	-0.084	-0.021	0.038	-0.124	-11.8743
Field=20	0.766	-0.182	-0.081	-0.027	0.043	-0.128	-14.2445
Field=25	0.766	-0.186	-0.079	-0.033	0.048	-0.132	-16.7107

increases with the increase of electric field strength. This phenomenon suggests that the electric field can strengthen the electron-donating capability of the Zn-porphyrin and phenyl groups, and thus enhance the performance of DSSC.

Unfortunately, for dye C system, the EPS has no change for dye C system under different electric field strength. The negative charges are also located on tetrapyrrole macrocycle and the O atom of the carboxyl group for all dye C systems, and the positive charges are mainly located on phenyl groups and the H atom of the carboxyl group. Interestingly, different from the above two systems, there are no obvious positive charges on Zn^{2+} cation. Overall, the inner electric field still has little effect on the dye C system.

The natural bond orbital (NBO) charges on the six atoms lie in x-axis, parallel to the electric direction in dye A systems under different electric field strengths are listed in Table 4. From Table 4, the NBO charges on atom C_1 have no obvious change adjusting the electric field strength. As for other atoms, the charge on C_3 and C_5 atoms increase, while the charges on C_2, C_4 and C_6 atoms decrease along with increasing electric field strength. The dye A and B systems (see Supplementary Table S14) showed the same change trend. While, no matter how much the field strength is, the NBO charges almost have no change for the dye C system (see Supplementary Table S15). It indicates that the charge distribution is not affected by the internal electric field.The x-axis components of the inherent dipole moment of dye A, B and C systems without electric field are -5.1421, -4.4161 and 4.1342 D, respectively. When the inner electric field is applied, the electron density distribution is broken and leads to a change of dipole moment. The direction of induced dipole moment is immobile and the value of dipole moment is increased with increasing electric field for dye A and B systems in the field range used. As for dye C systems, the value of dipole moment is decreased with increasing electric field and the direction of induced dipole moment is immobile. But, we think that when the inner electric field strength continues to increase, the dipole direction may be reversed.

3.6 Theoretical understanding of the efficiency of three types of Zn-porphyrin sensitizers with inner electric field in DSSC

Now we assess the performance of the three type Zn-porphyrin sensitizers with and without an inner electric field in solar cells from a theoretical point of view. We have provided some reasonable explanation on the influence of the inner electric field on the efficiency of the DSSCs. To gain insight of the efficiency of different type Zn-porphyrin sensitizer under the different electric field, the properties of photo-current and photo-voltage were simulated in this work. In order to evaluate the photo-current and photo-voltage performance of different type Zn-porphyrin sensitizer, the next two criteria are used to set up an effective ranking: (1) the key parameters (ΔG^{inject}, ΔG^{reg} and *LHE*) of dye should have to be as large as possible so as to enlarge J_{sc}; (2) raising the TiO_2 conduction band edge to increase the V_{oc}.

A key factor related to the efficiency of DSSC is the performance of the sensitizer without an inner electric field in responsibility to the incident light. Based on the *LHE* of the dye, the value has to be as high as possible to maximize the photocurrent response. In this work, Peak Area calculation method that we used is more precise and accurate than the maximum absorption method because it cover all excited state transitions, even low-intensity transitions, and quantitative study would be possible. Moreover, this method has been successfully used in previous work.[18, 19] The Peak Area for all systems has been calculation and listed in Table 5. For all systems, the Peak Area is calculated through following equation:

$$A\% = \frac{A - A_{ref}}{A_{ref}} \quad (9)$$

Taking into account the actual operation conditions of the DSSCs, the Peak Area for the dye-TiO_2 system without an inner electric field in THF solution is selected to serve as an A-reference (A_{ref}) for different type sensitizers. As it is observable from the data in Table 5, the Peak Area is increased with the increasing electric field strength, which is a result of peak broadening and red-shifted for dye A system. It indicates that the dye A sensitizer under inner electric field has more efficient

Table 5 Numerical values for Peak Area and the X-axial dipole moment components of the adsorbed ($\mu_{x\text{-}ads}$) for the dye A, B and C system with different electric field strengths. (The A is the Absorption Peak Area of dye A, B and C system with and without different local electric strengths. The A_{ref} is the Absorption Peak Area for the dye A, B and C system without inner electric field. The ΔA is the difference of Absorption Peak Area between A and A_{ref}. Moreover, the A% is the ratio of ΔA to A_{ref}.)

System	Field (10^{-4} a.u.)	A	ΔA	A%	$\mu_{x\text{-}ads}$ (Debye)
A	0	76.59	—		34.6638
	5	118.54	41.59	54.77	31.5724
B	0	134.45	—		37.1582
	5	120.82	-13.63	-10.14	34.4730
C	0	33.52	—		30.0604
	5	25.77	-7.75	-23.12	27.5659

LHE as compared to the off-field condition. Thus, we can conclude that the electric field can lead to high photon to current response than that to the off-field condition. However, contrary to the A system, the Peak Area of dye B and C systems are decreased with the increasing electric field strength. Hence, these phenomena lead to a low *LHE* value.

In addition, the driving force of the electron injection (ΔG^{inject}) is an important property that could help increase the J_{sc} values. Thus, the electronic injection free enthalpy ΔG^{inject}, ground (E^{dye}) and excited state (E^{dye*}) oxidation potentials computed for the A sensitizer under different electric field are summarized in Table 6 and Fig. 8.

The ground state oxidation potential (GSOP) is related to the total electron attachment energy in solution. The rigorous way to obtain the GSOP (ΔG_{ox}) is to compute free energy different between the neutral and the oxidized ground-state species, (G^0-G^+)$_{GS}$.[49] The Gibbs free energy in solution of a species i (G^i_{solv}) is defined as:

$$G^i_{solv} = G^i_{vac} + \Delta G^i_{solv} \quad (10)$$

where G^i_{vac} is the Gibbs free energy in gas phase and ΔG^i_{solv} is the free energy of solution. This method requires the inclusion of the translational, rotational, and vibrational contribution to the total partition function, which is computationally more accurate. As can be seen from the data in Fig. 8, the energies of E^{dye}, $E_{0\text{-}0}$ and E^{dye*} are decreased for dye A and B systems (see Supplementary Table S16) with the increasing electric field strength, which is a result of small ΔG^{inject} and large ΔG^{reg}. We think the inner electric field has a moderating effect on sensitizer energies, and this effect is mutual; on the one hand, the electric field can affect the values of ΔG^{inject} and ΔG^{reg}, thereby affecting the J_{sc}, on the other hand, the intensity of J_{sc} can influence the electric field strength. In general, the value of ΔG^{inject} should be at least ~ 0.5 eV higher than the E_{CB} has recommended by Grätzel for efficient solar energy-to-current conversion.[50] And, in order to have an efficient dye regeneration process, the ΔG^{reg} should be about 0.2 eV.[51, 52] Although the value of ΔG^{inject} decreases, it can still guarantee the efficient electron injection process and reduce unnecessary waste of excited energy. At the same time, the increasing of ΔG^{reg} value can guarantee the successful completion of the

Table 6 The electronic injection free enthalpy ΔG^{inject} (eV), ground E^{dye} (eV) and excited E^{dye*} (eV) state oxidation potentials, the calculated transition energy $E_{0\text{-}0}$ (eV) and dye regeneration ΔG^{reg} of dye A system.

Field (10^{-4} a.u.)	E^{dye} (eV)	$E_{0\text{-}0}$ (eV)	E^{dye*} (eV)	ΔG^{inject} (eV)	ΔG^{reg} (eV)
Field=0	-4.87	2.07	-2.80	1.20	0.07
Field=5	-4.94	2.06	-2.88	1.12	0.14
Field=10	-5.00	2.04	-2.96	1.04	0.20
Field=15	-4.98	2.01	-2.97	1.03	0.18
Field=20	-5.03	2.00	-3.03	0.97	0.23
Field=25	-5.07	1.90	-3.17	0.88	0.27

sensitizer regeneration process. Also, we believe that this interaction will reach equilibrium state; this would be a time of the best performance of sensitizer. Moreover, for dye C system (see Supplementary Table S17), the energies of $E_{0\text{-}0}$ and E^{dye*} are decreased, and the energies of E^{dye} have no change. This situation has led to the gradual decreases of ΔG^{reg} constant and ΔG^{inject}. Hence, the effect of the internal electric field on the C system is disadvantageous to the efficiency of DSSCs.

As discussed in this section, we know that besides the short-circuit current density J_{sc} the overall power conversion efficiency also could be influenced by the open-circuit voltage V_{oc}. The shift in the conduction band of the semiconductor could lead to an increase in the Voc. This shift can be assessed based on the increase in the μ_{normal} of the adsorbed molecules pointing outward from the semiconductor surface. In this work, we utilized $\mu_{x\text{-}ads}$ symbol instead of μ_{normal} to distinguish it from the dipole moment of bare dyes ($\mu_{x\text{-}bare}$). As shown in Table 5, the variation trend of the $\mu_{x\text{-}ads}$ for the three types of Zn-porphyrin sensitizers are the same, namely, the dipole moment along the direction of the x-axis gradually decreases as increasing the electric field strength. All systems have larger μ values under electric field condition compare to the off-field condition. This infers that all the Zn-porphyrin sensitizers with electric field would likely shift the CB of the semiconductor toward the vacuum energy level, thus producing qualitatively higher V_{oc} values. As a consequence, we could draw a conclusion that the appropriate ΔG^{inject} and ΔG^{reg} with large *LHE* and V_{oc} have a high efficiency. Thus, the performance of DSSCs sensitized by dye A with inner electric field might superior to that dye B under the on-field condition, due to its favorable performances of the above factors based on our computed results. Moreover, according to our calculation results, the C system have the worst performance parameters, which may be the reason why the low efficiency of this kind of dye.

4. Conclusion

In this work, theoretical calculations have been performed on the three Zn-porphyrin sensitizer systems under the different electric fields to reveal the electronic structures, optical properties, focusing on the theoretical understanding of their performance as sensitizers in DSSC. The calculation results indicate that the inner electric field is a crucial factor which affects the electron density distribution, electron transition nature, and the electron transport activity in DSSC. Meanwhile,

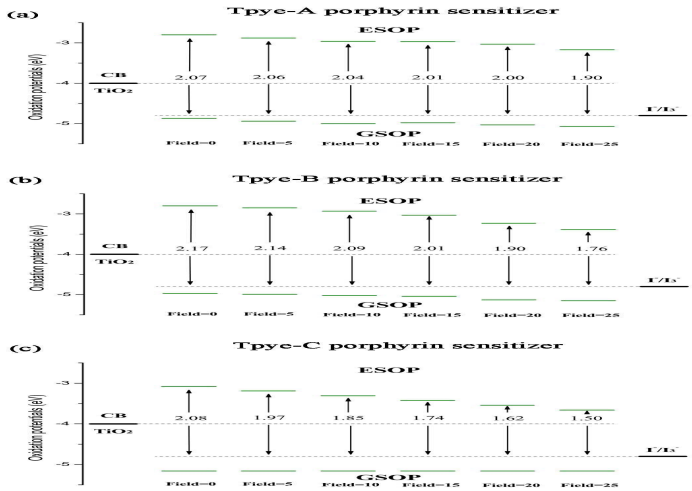

Fig. 8. Theoretical oxidation potentials (eV) of dye A, B and C with different electric field strengths. The band gap was based on the E0-0 transition in THF solution.

the effects of the inner electric field on the different structure of sensitizer molecules are also different. Although the inner electric field has great influence on its photoelectric properties, some key parameters are not as good as the dye A system. In the end, the inner electric field has little effect on the dye C system, even there is also a disadvantage. This may become a factor in their general efficiency.

Among all systems, the *meso*-substituted Zn-porphyrin sensitizer (dye A system) under on-field condition would perform more efficiently than under any off-field condition according to the calculated key parameters (ΔG^{inject}, ΔG^{reg}, *LHE* and ΔE_{cb}). Inspection of the frontier MOs of the dye A system absorbed onto TiO_2 film also indicates larger orbital-coupling strength in the on-field condition, which will facilitate electron injection from dye to the CB of TiO_2. Therefore, we believe that the dye A system has self-promoting properties. Namely, when the A dye is used in DSSC, the inner electric field generated will increase the dye property, which in turn will produce stronger electric field strength, and finally reach the equilibrium. This may be one of the reasons that the *meso*-substituted Zn-porphyrin sensitizers have the highest efficiency. Overall, our calculated results demonstrate that it is the key for molecular engineering aspect of molecular design, which can adjust the inner electric field strength and raise the performance of the dye molecule and DSSCs. These results should be helpful for establishing the relationships of molecular structure and efficiency, and to deepen the understanding of the operation mechanism of DSSCs in detail.

Acknowledgements

This work was supported by the Natural Science Foundation of China (Grant No. 21173096) and the State Key Development Program for Basic Research of China (Grant No. 2013CB834801) and Ningbo University Research Programs (Grant No. 421600710) and K. C. Wong Magna Fund in Ningbo University.

Notes and references

1. T. W. Hamann, R. A. Jensen, A. B. F. Martinson, H. Van Ryswyk and J. T. Hupp, *Energy & Environmental Science*, 2008, 1, 66-78.
2. M. Gratzel, *Nature*, 2001, 414, 338-344.
3. B. O'Regan and M. Gratzel, *Nature*, 1991, 353, 737-740.
4. M. K. Nazeeruddin, A. Kay, I. Rodicio, R. Humphry-Baker, E. Mueller, P. Liska, N. Vlachopoulos and M. Graetzel, *Journal of the American Chemical Society*, 1993, 115, 6382-6390.
5. M. K. Nazeeruddin, S. M. Zakeeruddin, R. Humphry-Baker, M. Jirousek, P. Liska, N. Vlachopoulos, V. Shklover, C.-H. Fischer and M. Grätzel, *Inorganic Chemistry*, 1999, 38, 6298-6305.
6. P. Péchy, T. Renouard, S. M. Zakeeruddin, R. Humphry-Baker, P. Comte, P. Liska, L. Cevey, E. Costa, V. Shklover, L. Spiccia, G. B. Deacon, C. A. Bignozzi and M. Grätzel, *Journal of the American Chemical Society*, 2001, 123, 1613-1624.
7. A. Yella, H.-W. Lee, H. N. Tsao, C. Yi, A. K. Chandiran, M. K. Nazeeruddin, E. W.-G. Diau, C.-Y. Yeh, S. M. Zakeeruddin and M. Grätzel, *Science*, 2011, 334, 629-634.
8. S. Mathew, A. Yella, P. Gao, R. Humphry-Baker, B. F. Curchod, N. Ashari-Astani, I. Tavernelli, U. Rothlisberger, M. K. Nazeeruddin and M. Grätzel, *Nature chemistry*, 2014, 6, 242-247.
9. W. Zeng, Y. Cao, Y. Bai, Y. Wang, Y. Shi, M. Zhang, F. Wang, C. Pan and P. Wang, *Chemistry of Materials*, 2010, 22, 1915-1925.
10. M. Zhang, Y. Wang, M. Xu, W. Ma, R. Li and P. Wang, *Energy & Environmental Science*, 2013, 6, 2944-2949.
11. K. Ladomenou, T. Kitsopoulos, G. Sharma and A. Coutsolelos, *Rsc Advances*, 2014, 4, 21379-21404.

12. M. Ishida, S. W. Park, D. Hwang, Y. B. Koo, J. L. Sessler, D. Y. Kim and D. Kim, *The Journal of Physical Chemistry C*, 2011, 115, 19343-19354.
13. J. K. Park, H. R. Lee, J. Chen, H. Shinokubo, A. Osuka and D. Kim, *The Journal of Physical Chemistry C*, 2008, 112, 16691-16699.
14. M. T. Brumbach, A. K. Boal and D. R. Wheeler, *Langmuir*, 2009, 25, 10685-10690.
15. C. F. Negre, R. L. Milot, L. A. Martini, W. Ding, R. H. Crabtree, C. A. Schmuttenmaer and V. S. Batista, *The Journal of Physical Chemistry C*, 2013, 117, 24462-24470.
16. H. B. Gobeze, S. K. Das and F. D'Souza, *The Journal of Physical Chemistry C*, 2014, 118, 16660-16671.
17. M. Xie, J. Wang, J. Ren, L. Hao, F.-Q. Bai, Q.-J. Pan and H.-X. Zhang, *Organic Electronics*, 2015, 26, 164-175.
18. M. M. Waskasi, S. M. Hashemianzadeh and O. M. Sarhangi, *Computational and Theoretical Chemistry*, 2011, 978, 33-40.
19. O. M. Sarhangi, S. M. Hashemianzadeh, M. M. Waskasi and A. P. Harzandi, *Journal of Photochemistry and Photobiology A: Chemistry*, 2011, 225, 95-105.
20. U. B. Cappel, E. A. Gibson, A. Hagfeldt and G. Boschloo, *The Journal of Physical Chemistry C*, 2009, 113, 6275-6281.
21. U. B. Cappel, S. M. Feldt, J. Schöneboom, A. Hagfeldt and G. Boschloo, *Journal of the American Chemical Society*, 2010, 132, 9096-9101.
22. W. Yang, M. Pazoki, A. I. Eriksson, Y. Hao and G. Boschloo, *Physical Chemistry Chemical Physics*, 2015, 17, 16744-16751.
23. M. J. Frisch, Trucks, G.W., Schlegel, H.B., Scuseria, G.E., Robb, M.A., Cheeseman, J.R., Scalmani, G., Barone, V., Mennucci, B., Petersson, G.A., Nakatsuji, H., Caricato, M., Li, X., Hratchian, H.P., Izmaylov, A.F., Bloino, J., Zheng, G., Sonnenberg, J.L., Hada, M., Ehara, M., Toyota, K., Fukuda, R., Hasegawa, J., Ishida, M., Nakajima, T., Honda, Y., Kitao, O., Nakai, H., Vreven, T., Montgomery, J.A., Jr., Peralta, J.E., Ogliaro, F., Bearpark, M., Heyd, J.J., Brothers, E., Kudin, K.N., Staroverov, V.N., Kobayashi, R., Normand, J., Raghavachari, K., Rendell, A., Burant, J.C., Iyengar, S.S., Tomasi, J., Cossi, M., Rega, Millam, N.J., Klene, M., Knox, J.E., Cross, J.B., Bakken, V., Adamo, C., Jaramillo, J., Gomperts, R.E., Stratmann, O., Yazyev, A.J., Austin, R., Cammi, C., Pomelli, J.W., Ochterski, R., Martin, R.L., Morokuma, K., Zakrzewski, V.G., Voth, G.A., Salvador, P., Dannenberg, J.J., Dapprich, S., Daniels, A.D., Farkas, O., Foresman, J.B., Ortiz, J.V., Cioslowski, J., Fox, D.J., 2009. Gaussian 09, Revision D.01. Gaussian, Inc., Wallingford CT.
24. A. D. Becke, *The Journal of Chemical Physics*, 1993, 98, 5648-5652.
25. M. Xie, J. Wang, H.-Q. Xia, F.-Q. Bai, R. Jia, J.-G. Rim and H.-X. Zhang, *RSC Advances*, 2015, 5, 33653-33665.
26. M. E. Casida, C. Jamorski, K. C. Casida and D. R. Salahub, *The Journal of Chemical Physics*, 1998, 108, 4439-4449.
27. N. N. Matsuzawa, A. Ishitani, D. A. Dixon and T. Uda, *The Journal of Physical Chemistry A*, 2001, 105, 4953-4962.
28. R. E. Stratmann, G. E. Scuseria and M. J. Frisch, *The Journal of Chemical Physics*, 1998, 109, 8218-8224.
29. V. Barone, M. Cossi and J. Tomasi, *The Journal of Chemical Physics*, 1997, 107, 3210-3221.
30. B. Mennucci and J. Tomasi, *The Journal of Chemical Physics*, 1997, 106, 5151-5158.
31. T. Lu and F. Chen, *Journal of Computational Chemistry*, 2012, 33, 580-592.
32. M. R. Narayan, *Renewable and Sustainable Energy Reviews*, 2012, 16, 208-215.
33. J. Zhang, H.-B. Li, S.-L. Sun, Y. Geng, Y. Wu and Z.-M. Su, *Journal of Materials Chemistry*, 2012, 22, 568-576.
34. W. Sang-aroon, S. Saekow and V. Amornkitbamrung, *Journal of Photochemistry and Photobiology A: Chemistry*, 2012, 236, 35-40.
35. R. Katoh, A. Furube, T. Yoshihara, K. Hara, G. Fujihashi, S. Takano, S. Murata, H. Arakawa and M. Tachiya, *The Journal of Physical Chemistry B*, 2004, 108, 4818-4822.
36. J. Feng, Y. Jiao, W. Ma, M. K. Nazeeruddin, M. Grätzel and S. Meng, *The Journal of Physical Chemistry C*, 2013, 117, 3772-3778.
37. S. G. Boxer, *The Journal of Physical Chemistry B*, 2009, 113, 2972-2983.
38. G. U. Bublitz and S. G. Boxer, *Annual Review of Physical Chemistry*, 1997, 48, 213-242.
39. M. Lazzeri, A. Vittadini and A. Selloni, *Physical Review B*, 2001, 63, 155409.
40. J. Chen, F.-Q. Bai, J. Wang, L. Hao, Z.-F. Xie, Q.-J. Pan and H.-X. Zhang, *Dyes and Pigments*, 2012, 94, 459-468.
41. Y.-X. Weng, L. Li, Y. Liu, L. Wang and G.-Z. Yang, *The Journal of Physical Chemistry B*, 2003, 107, 4356-4363.
42. Y. Xie, Y. Tang, W. Wu, Y. Wang, J. Liu, X. Li, H. Tian and W. H. Zhu, *J Am Chem Soc*, 2015, 137, 14055-14058.
43. Y. Tang, Y. Wang, X. Li, H. Agren, W. H. Zhu and Y. Xie, *ACS applied materials & interfaces*, 2015, 7, 27976-27985.
44. H. H. Chou, K. S. Reddy, H. P. Wu, B. C. Guo, H. W. Lee, E. W. Diau, C. P. Hsu and C. Y. Yeh, *ACS applied materials & interfaces*, 2016, 8, 3418-3427.
45. T. Le Bahers, C. Adamo and I. Ciofini, *Journal of chemical theory and computation*, 2011, 7, 2498-2506.
46. I. Ciofini, T. Le Bahers, C. Adamo, F. Odobel and D. Jacquemin, *The Journal of Physical Chemistry C*, 2012, 116, 11946-11955.
47. D. Jacquemin, T. Le Bahers, C. Adamo and I. Ciofini, *Physical Chemistry Chemical Physics*, 2012, 14, 5383-5388.
48. T. Le Bahers, E. Brémond, I. Ciofini and C. Adamo, *Physical Chemistry Chemical Physics*, 2014, 16, 14435-14444.
49. C.-R. Zhang, Z.-J. Liu, Y.-H. Chen, H.-S. Chen, Y.-Z. Wu, W. Feng and D.-B. Wang, *Current Applied Physics*, 2010, 10, 77-83.

50. M. Grätzel, *Accounts of chemical research*, 2009, 42, 1788-1798.
51. M. Pastore, S. Fantacci and F. De Angelis, *The Journal of Physical Chemistry C*, 2010, 114, 22742-22750.
52. G. Boschloo and A. Hagfeldt, *Accounts of Chemical Research*, 2009, 42, 1819-1826.

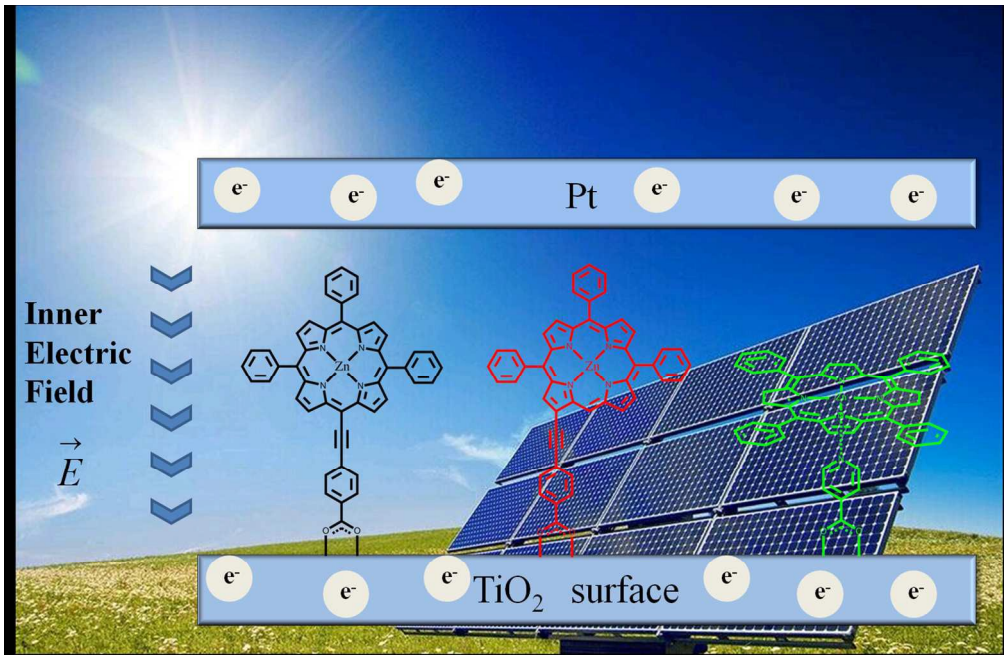

257x166mm (150 x 150 DPI)